Excess entropy and crystallization in Stillinger-Weber and Lennard-Jones fluids

ARTICLE *in* THE JOURNAL OF CHEMICAL PHYSICS · OCTOBER 2015

Impact Factor: 2.95 · DOI: 10.1063/1.4933420

Excess entropy and crystallization in Stillinger-Weber and Lennard-Jones fluids

Debdas Dhabal, Andrew Huy Nguyen, Murari Singh, Prabir Khatua, Valeria Molinero, Sanjoy Bandyopadhyay , and Charusita Chakravarty

Citation: The Journal of Chemical Physics **143**, 164512 (2015); doi: 10.1063/1.4933420
View online: http://dx.doi.org/10.1063/1.4933420
View Table of Contents: http://scitation.aip.org/content/aip/journal/jcp/143/16?ver=pdfcov
Published by the AIP Publishing

Excess entropy and crystallization in Stillinger-Weber and Lennard-Jones fluids

Debdas Dhabal,[1] Andrew Huy Nguyen,[2] Murari Singh,[3] Prabir Khatua,[4] Valeria Molinero,[2] Sanjoy Bandyopadhyay,[4] and Charusita Chakravarty[1,a)]
[1]*Department of Chemistry, Indian Institute of Technology Delhi, New Delhi 110016, India*
[2]*Department of Chemistry, University of Utah, Salt Lake City, Utah 84112-0850, USA*
[3]*Department of Chemical Physics, Weizmann Institute of Science, Rehovot 76100, Israel*
[4]*Department of Chemistry, Indian Institute of Technology Kharagpur, Kharagpur 721302, India*

(Received 19 August 2015; accepted 7 October 2015; published online 29 October 2015)

Molecular dynamics simulations are used to contrast the supercooling and crystallization behaviour of monatomic liquids that exemplify the transition from simple to anomalous, tetrahedral liquids. As examples of simple fluids, we use the Lennard-Jones (LJ) liquid and a pair-dominated Stillinger-Weber liquid (SW_{16}). As examples of tetrahedral, water-like fluids, we use the Stillinger-Weber model with variable tetrahedrality parameterized for germanium (SW_{20}), silicon (SW_{21}), and water ($SW_{23.15}$ or mW model). The thermodynamic response functions show clear qualitative differences between simple and water-like liquids. For simple liquids, the compressibility and the heat capacity remain small on isobaric cooling. The tetrahedral liquids in contrast show a very sharp rise in these two response functions as the lower limit of liquid-phase stability is reached. While the thermal expansivity decreases with temperature but never crosses zero in simple liquids, in all three tetrahedral liquids at the studied pressure, there is a temperature of maximum density below which thermal expansivity is negative. In contrast to the thermodynamic response functions, the excess entropy on isobaric cooling does not show qualitatively different features for simple and water-like liquids; however, the slope and curvature of the entropy-temperature plots reflect the heat capacity trends. Two trajectory-based computational estimation methods for the entropy and the heat capacity are compared for possible structural insights into supercooling, with the entropy obtained from thermodynamic integration. The two-phase thermodynamic estimator for the excess entropy proves to be fairly accurate in comparison to the excess entropy values obtained by thermodynamic integration, for all five Lennard-Jones and Stillinger-Weber liquids. The entropy estimator based on the multiparticle correlation expansion that accounts for both pair and triplet correlations, denoted by S_{trip}, is also studied. S_{trip} is a good entropy estimator for liquids where pair and triplet correlations are important such as Ge and Si, but loses accuracy for purely pair-dominated liquids, like LJ fluid, or near the crystallization temperature (T_{thr}). Since local tetrahedral order is compatible with both liquid and crystalline states, the reorganisation of tetrahedral liquids is accompanied by a clear rise in the pair, triplet, and thermodynamic contributions to the heat capacity, resulting in the heat capacity anomaly. In contrast, the pair-dominated liquids show increasing dominance of triplet correlations on approaching crystallization but no sharp rise in either the pair or thermodynamic heat capacities. © *2015 AIP Publishing LLC.* [http://dx.doi.org/10.1063/1.4933420]

I. INTRODUCTION

Phase transformations and liquid state behaviour of simple liquids are dominated by pair correlations and the relationships between structural correlations, thermodynamic, and transport properties are fairly well-understood.[1–6] Simple liquids are exemplified by the model Lennard-Jones (LJ) fluid, though a wide range of atomic, molecular, and mesoscopic fluids fall in this category. Simple liquids can be mapped onto essentially hard- or soft-sphere fluids and are characterized by random, close-packing arrangements with a bias towards local icosahedral order. All liquids which are not simple are termed as complex fluids.

One can consider the simplest category of complex fluids to be created by introducing three-body or triplet correlations which reflect a locally anisotropic environment for the fluid particles. Tetrahedral fluids fall in this class of the simplest of complex fluids and include a number of important systems, such as water,[7,8] ionic melts (SiO_2, BeF_2),[3,9–15] covalently bonded liquids (C, Si),[16–21] metalloids (Ge, Sn),[22,23] and dispersions of patchy colloids.[24,25] The characteristic feature of such tetrahedral liquids is a shift in local order from relatively open, tetrahedral packing at low densities and temperatures to more random, close-packing arrangements similar to simple liquids at high temperatures and densities. Depending on the degree of bias towards tetrahedrality, such systems

a)Author to whom correspondence should be addressed. Electronic mail: charus@chemistry.iitd.ac.in. Tel.: (+)91-11-2659-1510. Fax: (+)91-11-4716-5550.

show a number of anomalies when compared to simple liquids, such as rise in density on isobaric heating, sharp rise in compressibility and heat capacity on isobaric cooling, negative volume changes on melting, and crystalline polymorphism and polyamorphism.[3,19,22,26] Since water is the best-known and most important tetrahedral liquid, this set of anomalies is frequently referred to collectively as "water-like" anomalies. The Stillinger-Weber (SW) family of liquids of variable tetrahedrality has been shown to be a very convenient model that captures much of the complex phenomenology of the transition from simple to anomalous, water-like behaviour.[19–21,26–31] The Stillinger-Weber potential was originally developed to model silicon with configurational energy, U written as the sum of a two-body term, ϕ_2, and a three-body term, ϕ_3, imposing an energetic penalty for deviations from local tetrahedrality. This basic parametric form was generalized as

$$U = \sum_{\substack{\text{unique}\\ \text{pairs}}} \phi_2 + \lambda \sum_{\substack{\text{unique}\\ \text{triplets}}} \phi_3 \qquad (1)$$

to create a family of liquids (SW_λ) with variable tetrahedrality controlled by the dimensionless parameter, λ. Figure 1 shows the phase diagram of this SW family of liquids in the tetrahedrality (λ)–temperature (T) plane. Appropriate reduced units for the SW liquids correspond to the well-depth (ϵ) and length scale (σ) associated with the pair interaction.[19,27,32] In their original study, Molinero *et al.* demonstrated that the ground crystalline structure of the SW liquids shifts from a body-centered cubic (bcc) to a tetrahedral diamond structure with increasing tetrahedrality.[19] The melting lines of the bcc and diamond crystal intersect at a pseudo-eutectic point ($\lambda \approx 18.75$) where the system adopts a β-tin structure. Strong glass-forming propensities were observed in the neighborhood of the eutectic. Moreover, by suitably tuning ϵ, σ, and λ, reasonable models of group IV elements like C, Si, Ge, and Sn were generated.[16–19,22,23,26,33,34] The SW model has also been adapted to generate a fairly versatile, coarse-grained monatomic water or mW model.[27,35–39] Some of the water-like anomalies, such as the density anomaly corresponding to a negative thermal expansion coefficient and negative volume change on melting, are pronounced at intermediate tetrahedralities and disappear in the limits of very high and low tetrahedrality. In contrast, the anomaly corresponding to the sharp rise in heat capacity on isobaric cooling exists for all SW liquids with the tetrahedral diamond ground state. For completeness, we note that the phenomenology of tetrahedral liquids described above is a consequence of energetic bias for tetrahedral coordination and is very different from that associated with packing of rigid tetrahedra.[40,41]

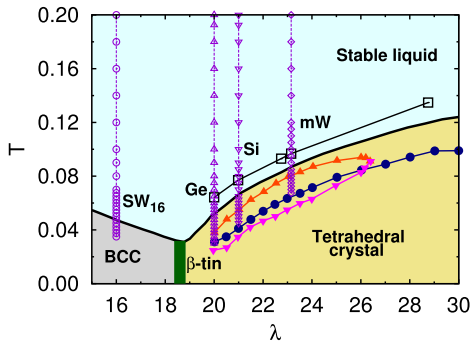

FIG. 1. Phase diagram of the Stillinger-Weber liquids in the tetrahedrality-temperature (λ-T) plane at zero pressure. Temperature is in reduced units with the depth of the pair potential serving as the unit of energy. The locus of points at which $S_2 = S_3$ is shown with open black squares and separates pair-dominated and triplet-dominated regimes is constructed with data from Ref. 32. The four SW systems for which we carry out isobaric quenching at a common reduced pressure of $P = 3.2269 \times 10^{-5}$ are shown by vertical violet lines, corresponding to monatomic water mW ($SW_{23.15}$), silicon (SW_{21}), germanium (SW_{20}) and a pair-dominated SW system with $\lambda = 16$ (SW_{16}). The locus of temperatures of maximum (TMD) and minimum density (TmD) is shown with red ($\triangle$) and pink (∇), respectively.[26] The line of heat capacity maxima is shown with filled, blue circles.[26] The melting line data are taken from previous publications.[19,27]

Simple liquids are characterised by strong pair correlations with icosahedral local order associated with random, close-packing of spheres.[42–45] Since the five-fold symmetry of icosahedral packing is incompatible with long-range translational order, therefore, such simple liquids crystallize into face-centred or hexagonal close packing for hard-spheres or body-centred close-packing for soft-sphere interactions, as seen for low-tetrahedrality SW liquids. As discussed above, with increasing tetrahedrality, local order in the solid as well as liquid state both shifts to anisotropic tetrahedral order. The degree of compatibility in local order between the solid and the liquid phases is known to result in characteristic differences in thermodynamics and kinetics of supercooling and crystallization of simple and tetrahedral liquids.[32,37,46] Using the multiparticle correlation expansion (MCE) of the fluid entropy to translate the information on pair and triplet correlations (see Section II B) into thermodynamic signatures, a recent study mapped out the total pair and triplet contributions to the entropy and heat capacity for the Stillinger-Weber liquids.[32] As shown in Figure 1, the set of state points in the λ-T plane for which the pair entropy, S_2, is equal to the triplet entropy, S_3, divides the liquid-phase into pair-dominated and triplet-dominated fluids. The pair-dominated fluids behave as simple liquids in terms of temperature-dependence of entropy, conformity to freezing rules, and a very weak rise in heat capacity on approaching the metastability limit of the liquid. The triplet-dominated liquids show a sharp rise in heat capacity as the metastability limit of the liquid is approached that is almost entirely due to structural reorganisation involving pair and triplet correlations. The phenomenology associated with the eutectic regime, such as strong, glass-forming tendencies, and the density and excess entropy anomalies can be attributed to the competition between pair and triplet correlations.

The motivation for this study is two-fold. The first aim is to understand the structural changes underlying the supercooling and crystallization behaviour of monatomic liquids that exemplify the transition from simple fluids to anomalous, water-like liquids. The second aim is to compare computational estimation methods for the two crucial thermodynamic quantities in this context, the entropy and the heat capacity. As examples of simple fluids, we use the Lennard-Jones liquid and the pair-dominated SW liquid with $\lambda = 16$ denoted by LJ and SW_{16}. As examples of tetrahedral fluids, we use the Stillinger-Weber models for germanium (SW_{20}), silicon (SW_{21}), and monatomic water ($SW_{23.15}$). Figure 1 shows the isobars along which each of these five systems is cooled; the melting temperatures (T_m)

TABLE I. Key data for Stillinger-Weber and Lennard-Jones liquids. Melting temperature, T_m, for SW and LJ liquids is taken from Refs. 19, 26, 27, 32, and 47. Threshold temperature below which the liquid crystallizes during a simulation run is denoted by T_{thr}. The temperatures of maximum density, T_{TMD}, are taken from Ref. 26. Temperatures are shown in reduced units for all systems and in kelvin for Ge(SW_{20}), Si(SW_{21}), and mW($SW_{23.15}$).

		SW			
	LJ	$\lambda = 16$	$\lambda = 20$	$\lambda = 21$	$\lambda = 23.15$
T_m	0.850	0.0472	0.0514	0.0659	0.0874
T_m (K)			1164.56	1658.97	272.34
T_{thr}	0.650	0.0350	0.0300	0.0450	0.0675
T_{thr} (K)			679.704	1132.83	210.33
T_{TMD}	...	...	0.0378	0.0546	0.0804
T_{TMD} (K)	...	...	856.427	1374.50	250.53

and the lower limit of liquid metastability (T_{thr}) are shown in Table I.[19,26,27] We focus on the two key thermodynamic quantities, entropy, S, and heat capacity, C_P that show characteristic signatures in the neighbourhood of phase transitions and also serve to distinguish between simple and water-like liquids.[32] The heat capacity anomaly has been described above. The total entropy, S, of a monatomic, classical fluid at temperature T and number density (ρ) can be written as the sum of the entropy of the corresponding ideal monatomic gas, S_{id}^{mono}, at the same T and ρ and an excess part, S_e, reflecting the lowering of entropy due to interactions and structural correlations as

$$S = S_{id}^{mono} + S_e. \tag{2}$$

The mass and Planck's constant dependence of the fluid entropy is contained entirely in the one-particle, ideal gas term, S_{id}^{mono}, while the excess entropy term, S_e, contains the effect of the interparticle interactions which give rise to pair and higher-order correlations in the fluid. The excess entropy proves to be a particularly useful quantity for relating structure, entropy, and transport properties of fluids.[3,48–51] A necessary condition for a fluid to show water-like thermodynamic and transport anomalies, such as the density anomaly, is the existence of an excess entropy anomaly where excess entropy rises on isothermal compression, $(\partial S_e/\partial \rho)_T > 0$. Excess entropy scaling of transport properties has been particularly useful from this point of view and explains why strong excess entropy anomalies are associated with mobility anomalies such as an increase in diffusivity on isothermal compression. For a given potential energy model of a fluid, free energy estimation methods such as Widom insertion and thermodynamic integration (TI) methods provide a simulation route to accurately measure thermodynamic quantities, including the entropy, within statistical error.[52–54] We use free energy estimation methods,[53] to estimate the thermodynamic entropy (S) and heat capacity (C_P) on supercooling of each of the five model fluids.

A large class of trajectory-based entropy estimation methods are available that relate averages of suitably defined functions of microscopic position and momentum variables to the thermodynamic entropy.[55–66] Such trajectory-based estimators are useful for providing microscopic insights into thermodynamic changes. We now compare S_e and C_P for the model fluids, as estimated by thermodynamic integration, with two of the currently widely used trajectory-based methods that seem to provide the most insight into the behaviour of fluids: the MCE method and the two-phase thermodynamic (2PT) method. The MCE approach writes the total entropy of the fluid as shown in Eq. (2) and expands the excess entropy, S_e, as

$$S_e = S_2 + S_3 + S_4 + S_5 + \cdots, \tag{3}$$

where S_n is the contribution due to n-particle correlations[63–70] to the entropy. The contribution of terms corresponding to different n need not necessarily decrease with increasing n but must reflect the actual structural correlations in the fluid. As the discussion above indicates, in simple fluids, the pair entropy term dominates and accounts for 85%-90% of the excess entropy in many systems.[66,68,71,72] Using the SW family of liquids, it can be shown that the transition from simple to tetrahedral, water-like liquids is driven by triplet correlations.[32] Thus, for the fluids considered in this study, the pair and triplet correlations to the excess entropy are crucial.

The 2PT method was originally formulated by Goddard and co-workers for Lennard-Jones fluids but has since been extended to many other liquids.[60,73–78] The key input for entropy estimation is the density of states (DOSs) function, obtained from Fourier transformation of the corresponding velocity auto-correlation function (VACF).[59–62,74,75,78] For a molecular fluid, such as water, the density of states function contains contributions from translational, rotational, and intramolecular vibrational modes of motion. In this study, we have selected both the simple and water-like fluids to be monatomic, and thus, the density of states function of the liquid will only have the translational contribution. As discussed below, the total liquid DOS, $DoS^{liquid}(\omega)$ can be partitioned into a gas-like contribution, $DoS^{gas}(\omega)$ based on the hard-sphere system and a solid-like component, $DoS^{solid}(\omega)$ based on harmonic phonon-modes of solids,[59]

$$DoS^{liquid}(\omega) = DoS^{gas}(\omega) + DoS^{solid}(\omega), \tag{4}$$

where ω refers to the frequency of normal modes. As discussed in Section II C, one can then develop an expression for the total fluid entropy, S^{2PT} by summing the contribution from hard-sphere and phonon components. The corresponding excess entropy will then be $S_e^{2PT} = S^{2PT} - S_{id}^{mono}$. As we show, comparison of the thermodynamic excess entropy (S_e) with these two trajectory-based estimators provides interesting insights into the links between structure and thermodynamics of fluids.

The paper is organised as follows. Section II describes the different entropy estimation methods used for the Stillinger-Weber and Lennard-Jones liquids in this study. Section III provides the computational details of the molecular dynamics simulations and entropy estimation methods used. Section IV discusses the results and Section V contains our conclusions.

II. ENTROPY ESTIMATION METHODS

A. Widom particle insertion method

The Widom insertion method to estimate the excess chemical potential was performed in both the isothermal-isobaric

(NPT) simulation as well as canonical (NVT) simulations.[53] To maintain correspondence with the isobaric cooling scenario, the mean volume obtained from the appropriate NPT simulation was used in the NVT simulations. The Widom insertion methods rely on random insertion of a test particle in the fluid under either NPT or NVT conditions such that ΔU is the potential energy of interaction of the test particle with the N particles constituting the ensemble. Note that no particle is actually added during the simulation and the ghost particle is identical in its interactions to those of the simulated fluid. The quantity, $\exp(-\Delta U/k_BT)$, corresponds to the probability of acceptance of a trial insertion. The accuracy of the Widom insertion method is best when the insertion probabilities are not too low, which corresponds to low-density/high-temperature states of fluids. In the NVT ensemble, the excess chemical potential, μ_e, can be computed using Widom insertion method with the following equation:[53,79]

$$\mu_e = -k_BT \ln\langle \exp(-\Delta U/k_BT)\rangle, \tag{5}$$

where $\langle \cdots \rangle$ denotes the ensemble average of the quantity within angular brackets. In the NPT ensemble, the excess chemical potential, μ_e, can be computed using Widom insertion method with the following equation:[53]

$$\mu_e = -k_BT \ln\left[\langle V \exp(-\Delta U/k_BT)\rangle/\langle V\rangle\right]. \tag{6}$$

Note that here V is instantaneous volume and $\langle V\rangle$ is the ensemble-averaged volume. The excess entropy is related to the excess chemical potential by[53]

$$S_e = (1/T)\left(\langle U\rangle - P_e\langle V\rangle - \mu_e\right). \tag{7}$$

1. TI method

Starting with the entropy at a state point calculated using a technique such as Widom particle insertion, the entropy at any other state point can be calculated, provided a suitable thermodynamic path can be constructed from the reference state to the state-point of interest which does not involve any phase changes or other singularities. Since this study uses NPT simulations to study supercooling along an isobar at pressure P, only the corresponding thermodynamic integration path is discussed. Defining the entropy at the reference state point by $S^{ref}(T^{ref}, P)$, the total entropy, $S(T, P)$ at any other temperature along the isobar, relative to the reference state point, can be obtained using

$$S(T,P) - S^{ref}(T^{ref},P) = \int_{T^{ref}}^{T} \frac{C_P}{T} dT. \tag{8}$$

We note that entropy $S^{ref}(T^{ref}, P)$ here denotes the total entropy of the fluid as

$$S^{ref}(T^{ref},P) = S_e^{ref}(T^{ref},P) + S_{id}^{ref}(T^{ref},P), \tag{9}$$

where $S_e^{ref}(T^{ref}, P)$ and $S_{id}^{ref}(T^{ref}, P)$ refer to the excess and ideal contribution to the entropy at the reference state point.

The ideal entropy $S_{id}(T, P)$ at any state point where the temperature is T and number density is $\rho = N/V$ can be calculated from the Sackur-Tetrode formula as

$$S_{id}/Nk_B = \ln\left[\frac{V}{N\Lambda^3}\right] + \frac{5}{2}, \tag{10}$$

where Λ is the thermal de-Broglie wavelength, $\Lambda = h/\sqrt{(2\pi m k_BT)}$, and h is Planck's constant. To evaluate the total entropy, we require the thermodynamic heat capacity at constant pressure, C_P. Heat capacity was calculated by two methods. The first method fitted the total enthalpy $H(T, P)$ along the isobar to a polynomial in T and differentiated to give $C_P = \left(\frac{\partial H}{\partial T}\right)_P$. The second method used the statistical fluctuation formula,[52]

$$C_P = \frac{1}{Nk_BT^2}\left(\langle H^2\rangle - \langle H\rangle^2\right). \tag{11}$$

Once the total entropy, $S(T, P)$ relative to the reference state, along an isobar is obtained, the corresponding ideal gas entropy $S_{id}(T, P)$ is subtracted to get excess entropy, $S_e(T, P)$. Note that the particle mass and Planck's constant enter only in the $S_{id}(T, P)$ formula and not in $S_e(T, P)$.

Isothermal compressibility is defined as fractional change in volume with respect to change in pressure at constant temperature

$$\kappa_T = -\frac{1}{V}\left(\frac{\partial V}{\partial P}\right)_T. \tag{12}$$

We can evaluate κ_T using the following fluctuation formula involving volume of the system in the NPT ensemble:[52]

$$\kappa_T = \frac{1}{\langle V\rangle k_BT}\left(\langle V^2\rangle - \langle V\rangle^2\right). \tag{13}$$

Thermal expansion coefficient is fractional change in volume with change in temperature at constant pressure,

$$\alpha_P = \frac{1}{V}\left(\frac{\partial V}{\partial T}\right)_P. \tag{14}$$

It can be calculated from the cross-correlations of enthalpy, H and volume, V of the system under NPT conditions using[52]

$$\alpha_P = \frac{1}{\langle V\rangle k_BT^2}\left(\langle VH\rangle - \langle V\rangle\langle H\rangle\right). \tag{15}$$

B. MCE approximation of excess entropy

We follow the notation of Hansen and McDonald[2] in defining the n-particle density and distribution functions in the canonical ensemble. For a system of N particles with positions given by $3N$-dimensional vector $\mathbf{r}^N$ and interaction potential $U(\mathbf{r}^N)$, the equilibrium n-particle density $\rho_N^{(n)}(\mathbf{r}^N)$ is the probability of finding n particles at n positions $(\mathbf{r}_1, \ldots, \mathbf{r}_n)$, irrespective of the positions of the remaining $(N - n)$ particles and irrespective of all momenta, and may be written as[2]

$$\rho_N^{(n)}(\mathbf{r}^n) = \frac{N!}{(N-n)!}\frac{1}{Z_N}\int \exp(-\beta U(\mathbf{r}^N))d\mathbf{r}^{(N-n)}, \tag{16}$$

where Z_N is the configurational integral given by $Z_N = \int \exp(-\beta U(\mathbf{r}^N))d\mathbf{r}^N$. Note that in Eq. (16), the integration is over $(N - n)$ coordinates unlike in the expression of configurational integral, Z_N, where integration is over all N position coordinates.

The n-particle correlation or distribution functions, $g_N^{(n)}(\mathbf{r}^n)$, provide a description of the structure of the fluids.

It is defined as

$$g_N^{(n)}(\mathbf{r}^n) = \frac{\rho_N^{(n)}(\mathbf{r}_1,\ldots,\mathbf{r}_n)}{\prod_{i=1}^{n}\rho_N^{(1)}(\mathbf{r}_i)}. \quad (17)$$

For a homogeneous, isotropic fluid, the lowest-order ($n = 1$) particle distribution function is

$$\rho_N^{(1)}(\mathbf{r}) = N/V = \rho, \quad (18)$$

where ρ is the number density of the system and the n-order correlation functions can be given by

$$\rho^n g_N^{(n)}(\mathbf{r}^n) = \rho_N^{(n)}(\mathbf{r}^n). \quad (19)$$

The $n = 2$ particle correlation function is the pair correlation function (PCF), $g_N^{(2)}(\mathbf{r}_1,\mathbf{r}_2)$, defined as

$$g_N^{(2)}(\mathbf{r}_1,\mathbf{r}_2) = \frac{N(N-1)}{\rho^2 Z_N}\int \exp(-\beta U(\mathbf{r}^N))d\mathbf{r}^{(N-2)}. \quad (20)$$

For a monatomic, homogeneous, isotropic fluid, the pair correlation function depends on only a single spatial variable, $r = r_{12} = |\mathbf{r}_2 - \mathbf{r}_1|$ and is denoted by $g^{(2)}(r)$. The atom-atom PCFs are directly accessible from X-ray and neutron scattering experiments and therefore have been extensively studied.[80–84] As discussed in the Introduction, they also dominate the structure and dynamics of simple liquids.

The triplet correlation function $g^{(3)}(\mathbf{r}_1,\mathbf{r}_2,\mathbf{r}_3)$ is the probability of observing any three particles at positions $\mathbf{r}_1$, $\mathbf{r}_2$, and $\mathbf{r}_3$ in the system. Following Eq. (16), we can write

$$g_N^{(3)}(\mathbf{r}_1,\mathbf{r}_2,\mathbf{r}_3) = \frac{N(N-1)(N-2)}{\rho^3 Z_N} \times \int \exp(-\beta U(\mathbf{r}^N))d\mathbf{r}^{(N-3)}. \quad (21)$$

For a homogeneous, isotropic fluid, it is obvious that the three mutual interparticle distances (r,s,t) where $r = |\mathbf{r}_2 - \mathbf{r}_1|$, $s = |\mathbf{r}_3 - \mathbf{r}_1|$, $t = |\mathbf{r}_3 - \mathbf{r}_2|$ are the most appropriate choice of spatial variables for representing variations in the triplet correlation function, which is denoted as $g^{(3)}(r,s,t)$. Note that since the three particles must form a triangle, the three scalar variables r, s, and t must satisfy the triangle inequality. The non-trivial contribution of triplet correlations is represented by irreducible part of the triplet correlation function, defined by

$$\delta g^{(3)}(\mathbf{r}_1,\mathbf{r}_2,\mathbf{r}_3) = \frac{g^{(3)}(\mathbf{r}_1,\mathbf{r}_2,\mathbf{r}_3)}{g^{(2)}(\mathbf{r}_1,\mathbf{r}_2)g^{(2)}(\mathbf{r}_2,\mathbf{r}_3)g^{(2)}(\mathbf{r}_3,\mathbf{r}_1)}. \quad (22)$$

The Kirkwood superposition approximation (KSA) corresponds to $\delta g^{(3)}(\mathbf{r}_1,\mathbf{r}_2,\mathbf{r}_3) = 1$, which assumes that the triplet correlation can be replaced by the product of the corresponding three pair correlations.

The ensemble invariant form of the multiparticle correlation expansion of the entropy was derived in a series of studies[63–66,69,85] originating with the work of Green in 1951. Here, we give the expressions for the first two terms in the series, the pair (S_2) and triplet (S_3) entropies for the monatomic fluids studied here. The pair correlation entropy can be written in terms of pair correlation function, $g^{(2)}(r)$ and number density, ρ as

$$S_2/Nk_B = -2\pi\rho\int_0^\infty \left[g^{(2)}(r)\ln g^{(2)}(r) - g^{(2)}(r) + 1\right]r^2 dr. \quad (23)$$

The triplet entropy S_3 can be defined as

$$\begin{aligned} S_3/Nk_B = &-\frac{\rho^2}{6}\int\int g^{(3)}(r,s,t)\ln \delta g^{(3)}(r,s,t)\mathbf{dr}\mathbf{ds} \\ &+ \frac{\rho^2}{6}\int\int \{g^{(3)}(r,s,t) - g^{(2)}(r)g^{(2)}(s) \\ &- g^{(2)}(s)g^{(2)}(t) - g^{(2)}(r)g^{(2)}(t) + g^{(2)}(r) \\ &+ g^{(2)}(s) + g^{(2)}(t) - 1\}\mathbf{dr}\mathbf{ds}. \end{aligned} \quad (24)$$

The relative magnitude of S_2 and S_3 terms indicates the relative weightage of pair and triplet correlation functions in determining thermodynamic behaviour, assuming that higher order correlations with $n > 3$ are negligible. In simple liquid, dominated by pair correlations, the S_2 term typically captures 85%–90% of the S_e.[32,66,68,71,72] The two- and three-body contributions to the heat capacity, denoted by C_2 and C_3, respectively, were calculated using the following equations:

$$C_2 = T\left(\frac{\partial S_2}{\partial T}\right)_P, \quad (25)$$

$$C_3 = T\left(\frac{\partial S_3}{\partial T}\right)_P. \quad (26)$$

For pair-dominated simple liquid, in the incompressible limit where $\kappa_T \approx 0$, Laird and Haymet proposed a useful approximation to estimate the excess entropy as[69,70]

$$S_{pair} = S_2 - (1/2), \quad (27)$$

which accounts for only pair correlations. An analogous expression was derived for liquids where both pair and triplet correlations are important in the incompressible limit by Singh *et al.*,[32]

$$S_{trip} = S_2 + S_3 - (1/3). \quad (28)$$

Thus, S_{pair} and S_{trip} may be viewed as approximations to the thermodynamic excess entropy, S_e, correct to second- and third-order in particle correlations.

C. 2PT method

This method involves calculating the density of states function from the Fourier transform of the corresponding velocity auto-correlation function. The liquid density of states $DoS^{liquid}(\omega)$ is partitioned into gas-like, $DoS^{gas}(\omega)$ and solid-like, $DoS^{solid}(\omega)$ components. Then the entropy, S^{2PT}, is written as integral of the density of state function weighted by the corresponding weighting function as[59,62]

$$S^{2PT} = k_B\left[\int_0^\infty DoS^{solid}(\omega)W^{solid}(\omega)d\omega + \int_0^\infty DoS^{gas}(\omega)W^{gas}(\omega)d\omega\right], \quad (29)$$

where the first term corresponds to the contribution due to the solid-like component and the second term corresponds to that of the gas-like component, and $W^{solid}(\omega)$ and $W^{gas}(\omega)$ are the respective weighting functions.

We first calculate total liquid DOS, $DoS^{liquid}(\omega)$ and DOS for gas-like component, $DoS^{gas}(\omega)$. As the systems we have chosen are monatomic, only the translational degrees of freedom are relevant. Thus, the total liquid DOS can be obtained from the Fourier transform of the mass-weighted linear VACF, $C_V(t)$, as

$$DoS^{liquid}(\omega) = \frac{2}{k_B T} \lim_{\tau\to\infty} \int_{-\tau}^{\tau} C_V(t) \exp(-i\omega t) dt, \quad (30)$$

with

$$C_V(t) = \sum_{i=1}^{N} m_i \langle \vec{\mathbf{v}}_i(0).\vec{\mathbf{v}}_i(t)\rangle, \quad (31)$$

where m_i is the mass of the ith particle and $\vec{\mathbf{v}}_i(t)$ is its velocity at time t. The DOS of gas-like component has been calculated using the hard sphere diffusive model as[59]

$$DoS^{gas}(\omega) = DoS^{HS}(\omega) = \frac{DoS^{liquid}(0)}{1 + \left[\frac{DoS^{liquid}(0)\omega}{12 f N}\right]^2}, \quad (32)$$

where $DoS^{liquid}(0)$ is the liquid DOS at zero frequency value and the parameter f is called the "fluidicity factor" which measures the fluidicity of the system. It has a limiting value from 0 to 1. For a hard-sphere gas $f = 1$, whereas for perfect solid $f = 0$. The fluidicity factor f is calculated using a universal expression as[60]

$$2\Delta^{-9/2} f^{15/2} - 6\Delta^{-3} f^5 - \Delta^{-3/2} f^{7/2} + 6\Delta^{-3/2} f^{5/2} + 2f - 2 = 0, \quad (33)$$

with Δ being the normalized diffusivity constant which is unitless and is a function of material properties and can be expressed as

$$\Delta(T, \rho, m, DoS^{liquid}(0)) = \frac{2DoS^{liquid}(0)}{9N} \times \left(\frac{\pi k_B T}{m}\right)^{1/2} \rho^{1/3} \left(\frac{6}{\pi}\right)^{2/3}, \quad (34)$$

with ρ as the number density of the system. Another quantity called hard-sphere packing fraction, y, relates with the normalized diffusivity, Δ, and fluidicity, f, as $f = \Delta(T, \rho, m, DoS^{liquid}(0))y^{2/3}$. Once we get the total DOS, $DoS^{liquid}(\omega)$ and DOS for the gas-like component, $DoS^{gas}(\omega)$, DOS for the solid-like component is just subtraction of these two quantities. Now to calculate the total entropy using Eq. (29), we need to determine the weighting functions for the solid-like and the gas-like components. The weighting function for the solid component $W^{solid}(\omega)$ can be calculated assuming each mode in the solid phase as a harmonic oscillator and expressed as

$$W^{solid}(\omega) = \frac{\beta\hbar\omega}{\exp(\beta\hbar\omega) - 1} - \ln\left[1 - \exp(-\beta\hbar\omega)\right]. \quad (35)$$

The weighting function for the gas phase component $W^{gas}(\omega)$ can be calculated using the hard sphere fluid model as

$$W^{gas}(\omega) = W^{HS}(\omega) = \frac{1}{3}\frac{S^{HS}}{k_B}, \quad (36)$$

where S^{HS} is hard-sphere entropy. Knowing f, the hard sphere entropy S^{HS} can be determined from the Carnahan-Starling equation of state[86] in terms of f and y,

$$S^{HS}/k_B = S^{IG}/k_B + \ln[z(fy)] + \frac{fy(3fy - 4)}{(1 - fy)^2}, \quad (37)$$

where S^{IG} is the ideal gas contribution to the entropy calculated at the corresponding temperature and density, z is the compressibility factor and can be calculated using the formula

$$z(y) = \frac{1 + y + y^2 - y^3}{(1 - y)^3}. \quad (38)$$

Once we get the total entropy, S^{2PT}, corresponding ideal gas entropy, S_{id} is subtracted to get the excess entropy, S_e^{2PT}. Note that ideal gas entropy was evaluated from Sackur-Tetrode formula given in Eq. (10). Heat capacity from 2PT entropy was calculated using the equation

$$C_P^{2PT} = T\left(\frac{\partial S^{2PT}}{\partial T}\right)_P. \quad (39)$$

III. SIMULATION DETAILS

A. Potential energy surface (PES)

1. Stillinger-Weber liquids

The parametric form of the Stillinger-Weber potential is written as a sum of two-body and three-body interaction term as given in Eq. (1). Here, ϕ_2 depends only on the relative separation of unique pairs of atoms and ϕ_3 depends on the relative distances between unique triplets as defined by two pair distances and the intervening angle. The tetrahedrality parameter which controls the energetic penalty for deviations from the tetrahedral angle, $\theta_0 = 109.47°$, is denoted by λ. Complete expressions for ϕ_2 and ϕ_3 are[17,27]

$$\phi_2(r_{ij}) = A\epsilon\left[B\left(\frac{\sigma}{r_{ij}}\right)^4 - 1\right]\exp\left(\frac{\sigma}{r_{ij} - a\sigma}\right), \quad (40)$$

$$\phi_3(r_{ij}, r_{ik}, \theta_{ijk}) = \epsilon(\cos\theta_{ijk} - \cos\theta_0)^2 \times \exp\left(\frac{\gamma\sigma}{r_{ij} - a\sigma}\right)\exp\left(\frac{\gamma\sigma}{r_{ik} - a\sigma}\right), \quad (41)$$

where the parameters are $A = 7.049\,556\,277$, $B = 0.602\,224\,558\,4$, $q = 0$, $\gamma = 1.20$, and $a = 1.80$. We used four λ values (16, 20, 21, and 23.15), of which three of them model real physical systems such as monatomic water ($\lambda = 23.15$), silicon ($\lambda = 21$), and germanium ($\lambda = 20$). For all SW liquids, a common set of reduced units can be defined using the particle mass (m), the length (σ), and energy (ϵ). In the molecular dynamics simulations discussed below, we use parameters in real units of the mW water model, i.e., $m = 18.02$ amu, $\sigma = 2.3925$ Å, and $\epsilon = 6.189$ kcal mol^{-1}, respectively. Unless otherwise stated, all results reported in this study are in reduced units.

2. Lennard-Jones liquid

The Lennard-Jones pair potential is given by

$$u_{LJ}(r) = 4\epsilon_{LJ}\left[\left(\frac{\sigma_{LJ}}{r}\right)^{12} - \left(\frac{\sigma_{LJ}}{r}\right)^{6}\right], \quad (42)$$

where ϵ_{LJ} is the well depth of the pair interaction and σ_{LJ} is the onset of the repulsive wall where $u_{LJ}(r) = 0$. As in the case of SW liquids, ϵ_{LJ} and σ_{LJ} can be used as reduced unit of energy and length, respectively. In the molecular dynamics simulations using Large-scale Atomic/Molecular Massively Parallel Simulator (LAMMPS) package,[87] standard parameters for argon, $\epsilon_{LJ} = 0.238\,067$ kcal mol^{-1}, $\sigma_{LJ} = 3.405$ Å, and molar mass, $m = 39.95$ amu were used. A cutoff distance of $4\sigma_{LJ}$ was used in the interaction potential and long range correction to the energy was included.

B. Molecular dynamics simulation

Molecular dynamics simulations of four SW liquids and one LJ liquid were carried out in the isothermal-isobaric (NPT) ensemble using the LAMMPS package.[87] All the simulations for SW liquids and LJ liquid were performed along reduced pressure, $P = 3.2269 \times 10^{-5}$ isobar and $P = 1.95$ isobar, respectively. The pressure and the temperature were maintained using Nose-Hoover thermostat and barostat, whose relaxation constants are given in Table III. The number of particles used in all the simulations was 4096, unless stated otherwise. The cubic periodic boundary conditions were used. The equations of motion were integrated using the velocity Verlet algorithm with a timestep of 5 fs for SW liquids and 2 fs for LJ liquid. Subsections III B 1–III B 4 describe simulation details for SW and LJ systems followed for computing excess entropy using different methods.

1. Excess entropy estimation using Widom insertion method

The excess chemical potential was computed using the Widom particle insertion method for all SW liquids. An initial 50 ns simulation at $P^{ref} = 3.2269 \times 10^{-5}$ was carried out at $T^{ref} = 0.180$ for $\lambda = 16$, $T^{ref} = 0.1925$ for $\lambda = 20$ and 21, and at $T^{ref} = 0.200$ for $\lambda = 23.15$ (see Table II). The average volume obtained from the NPT simulations was then used to carry out an NVT simulation in order to match the chemical potential values from the two ensembles. We used 2000 particle insertions every 10 steps for a total run length of 2×10^2 steps (10 ns). The difference in chemical potential obtained from the NPT runs and NVT runs was within statistical error. The chemical potentials obtained from NPT simulations were then used for computing excess entropies using Eq. (7) given in Section II A. For SW liquids with $\lambda = 16$ and 23.15, at a few selected temperatures, S_e was calculated along the P^{ref} isobar using Widom insertion method as a check on the thermodynamic integration procedure described in Sec. III B 2.

TABLE II. Data related to the entropy values at reference state point, T^{ref} and P^{ref} for SW and LJ liquids. In reduced units, $P^{ref} = 3.2269 \times 10^{-5}$ for SW liquids, while for LJ liquid $P^{ref} = 1.95$. The corresponding density at reference temperature (T^{ref}) and pressure (P^{ref}) is denoted by ρ^{ref}. The excess entropy at the reference state point is represented by S_e^{ref}. Ideal gas entropy S_{id}^{ref} in units of k_B was calculated using ρ^{ref} following the Sackur-Tetrode formula, $S_{id}^{ref} = \frac{5}{2} - \ln(\rho^{ref}\Lambda^3)$. Excess entropy value for LJ liquid at the reference point is taken from the literature.[47] Here, A is the acceptance percentage for test particle insertion in Widom method. Percentage error in excess entropy calculation for SW liquids using Widom insertion method at reference state point is given in the last row.

		SW			
	LJ	$\lambda = 16$	$\lambda = 20$	$\lambda = 21$	$\lambda = 23.15$
T^{ref}	0.8500	0.1800	0.1925	0.1925	0.2000
ρ^{ref}	0.8900	0.4913	0.4350	0.4240	0.3960
S_e^{ref}	−3.7485	−2.1784	−1.8658	−1.8253	−1.7017
S_{id}^{ref}	10.1798	11.080	11.302	11.3281	11.4536
A (%)	...	8.000	14.500	15.500	20.030
Error (%)	...	1.1700	1.3060	1.3330	1.4340

TABLE III. Molecular dynamics simulation details for SW and LJ liquids to calculate entropy using Widom, thermodynamic integration, 2PT and MCE methods. The number of particles used for each simulation is specified by N_{part}. The production run length is denoted by t_{prod}. Dumping frequency t_{dump} refers to the frequency at which enthalpy (for TI), coordinates (for MCE), coordinates and velocity both (for 2PT) were saved during MD simulation. Thermostat and barostat relaxation time constants used for the simulation are denoted by τ_t and τ_p, respectively.

System	Method	N_{part}	t_{prod} (ns)	t_{dump} (ps)	τ_t (ps)	τ_p (ps)
SW	Widom	4096	10	...	2.5	10
	TI	4096	50	0.5[a] 1.0[b]	1.0	10
	2PT	9216	0.05	0.005	0.1	2.0
	MCE	4096	50	5.0	1.0	10
LJ	TI	4096	10	0.2	0.5	1.0
	2PT	4096	0.16	0.002	0.5	1.0
	MCE	4096	10	1.0	0.5	1.0

[a] $\lambda = 16$ and 23.15.
[b] $\lambda = 20$ and 21.

2. Excess entropy estimation using TI method

Excess entropy S_e was calculated using TI method following the procedure given in Section II A 1 for the four SW liquids and one LJ liquid. The thermostat and barostat relaxation times for the NPT ensemble, the production run lengths, and the frequency at which the configurations are stored are given in Table III for both the systems. As the first step, the entropy at the reference state point for SW liquids was evaluated using Widom particle insertion method at $P^{ref} = 3.2269 \times 10^{-5}$ and the respective T^{ref} (given in Table II). The entropy at reference state point for LJ liquid is taken from Ref. 47. The entropy at any other state point relative to this reference state point was evaluated using Eq. (8). Since TI method involves fitting of enthalpy, $H(T, P^{ref})$, to a polynomial function of temperature, long production runs ensured good average values of $H(T, P^{ref})$ for both SW and LJ liquids.

We have evaluated the thermodynamic response functions such as isobaric heat capacity, C_P, isothermal compressibility, κ_T, and thermal expansion coefficient, α_P for both the systems using statistical fluctuation formula [see Eqs. (11), (13), and (15)]. These thermodynamic quantities were calculated by dividing the trajectory into 10 sub-trajectories and calculating average over all the sub-trajectories. The estimated errors in C_P, κ_T, and α_P were within 1%-6%.

3. Excess entropy estimation from 2PT method

The simulation details for SW liquids are described first. Each simulation of SW liquids consisted of 9216 particles in a cubic simulation box. Initially, a 10 ns long simulation was performed in the NPT ensemble with the Nose-Hoover temperature and pressure damping constants of 0.1 ps and 2.0 ps, respectively. After completion of each equilibration run, 5 ns NPT simulation was carried out during which restart files were saved every 500 ps. Using these ten restart files as the initial configuration, additional 50 ps NVT simulation was performed where the velocities and the coordinates of the particles were stored every 5 fs in order to calculate the 2PT entropy, S^{2PT}. The 2PT entropies S^{2PT} for all these 10 independent simulations were calculated and then the mean value was estimated. Once we get the S^{2PT}, the excess entropy, S_e^{2PT}, was calculated by subtracting the corresponding ideal gas entropy at the same temperature and density. As a check, for a single state point for mW system, the coordinates and velocities of atoms from the NVT runs were also stored every 1, 2, and 4 fs and the calculated entropy was found to be within the error bar.

For LJ liquid at each temperature, an initial 4 ns NPT simulation was performed. Then, a production run of 160 ps in NPT ensemble was carried out where the coordinates and velocities of atoms were stored every 2 fs. Each production run is then subdivided into eight parts to calculate the 2PT entropy, S^{2PT}. Mean value of the entropy and error bars was then calculated from these 8 sets of data. The molecular dynamics details associated with 2PT entropy estimation are summarised in Table III. To evaluate the 2PT approximation to the entropy, both the codes developed by Dr. Bandyopadhyay's group[62] and C++ code[59,60,76] developed by Goddard's group were used.

4. Evaluating pair and triplet correlation functions and entropies

The pair and triplet correlation functions and the corresponding entropies were evaluated along $P = 3.2269 \times 10^{-5}$ isobar for SW liquids and along $P = 1.95$ isobar for LJ liquid.

The pair correlation function $g^{(2)}(r)$ is computed by the standard methods[52,53] and the integral for the pair correlation entropy [see Eq. (23)] is evaluated to an upper limit of $L/2$, where L is the length of the cubical simulation box.

The procedure for computing triplet correlation function $g^{(3)}(r,s,t)$ is described briefly. For a single configuration from a simulation of N particles in a cubical box of length L, we first need to compute the elements of the histogram, where each element of the histogram, $A(r,s,t)$, corresponds to number of triplets that satisfy the requirement that the mutual distances lie in the range $r - \Delta$ to r, $s - \Delta$ to s, and $t - \Delta$ to t, with Δ being the histogram width. The triplet correlation function can then be written as

$$g^{(3)}(r,s,t) = \langle A(r,s,t)\rangle / V(r,s,t), \tag{43}$$

where $\langle A(r,s,t)\rangle$ is an ensemble average and $V(r,s,t)$ is the volume of the histogram bin. The histogramming of triplet distribution was adapted from Refs. 32, 88, and 89. The basic algorithm for histogramming is as follows:

- Considering each particle from a given configuration of an N particle system, $N - 1$ minimum image distances, R_{ij} are calculated. These $N - 1$ distances are then binned with an appropriate bin size Δ into a two-dimensional integer array, I_{ij}.
- Position of particle j relative to the particle i consistent with minimum image distances is stored in a companion array, C_{ij}.
- For a given particle i, two neighbours k and l are considered and assigned distances $r = I_{ik}$ and $s = I_{il}$ to create a triplet at the minimum image distances from particle i.
- The third mutual distance t between the particles l and k is calculated using the positions stored in the companion array elements, C_{ik} and C_{il}. Now update the element of histogram bin, $A(r,s,t)$ by one.

Due to the three dimensional nature of the triplet correlation function and triangle constraint, care should be taken during the computation of histogram volume. To compute the histogram volume, we followed the procedure given in Refs. 68 and 90. Calculation of triplet correlation entropy (S_3) was done using Eq. (24) given in Section II B. To maintain the triangle inequality and periodic boundary condition, the maximum range of integration limit must be kept as $L/4$, where L is the length of the cubical simulation box. Fluctuation in box length in NPT simulation should be considered in integration limit. Detailed checks on convergence of triplet entropy, S_3 for SW liquids were done in previous study.[32] For SW liquids, S_2 and S_3 values obtained from NPT and NVT simulations were found to agree.[32] The molecular dynamics simulation details and dumping frequency of coordinates are given in Table III.

IV. RESULTS AND DISCUSSIONS

We first consider the response function behaviour for isobaric cooling and crystallization of simple and water-like LJ and SW liquids studied here. Table I contains the melting temperatures of all the systems, taken from the literature.[26,27,32,47] The lowest temperature reached in the simulations before the liquid spontaneously crystallizes is termed the threshold temperature, T_{thr}, corresponding to the lower limit of liquid phase stability and is also shown in Table I. If rapid quenching, rather than equilibrium cooling, is carried out, then T_{thr} is marked by a heat capacity peak. Figure 2(a) shows the $C_P(T)$ curves for the five liquids, including state points in the crystallization regime with T less than T_{thr}. The LJ and pair-dominated SW_{16} show a negligibly very small rise in heat capacity on decrease in temperature consistent with simple liquid behaviour. In contrast, the water-like liquids show a pronounced, divergent rise in C_P on supercooling. The height of the peak in C_P or the degree of divergence increases as the degree of tetrahedrality increases (Ge < Si < mW).

Figure 2(b) shows the isothermal compressibility (κ_T) of the Stillinger-Weber and Lennard-Jones liquids on cooling along designated isobars from a fairly high temperature, to well below the melting temperature (T_m) till the lower limit of liquid phase stability at T_{thr} is reached. The $\kappa_T(T)$ plots provide a clear and qualitative distinction between simple and water-like liquids. The two simple liquids (LJ and SW_{16}) show a slow decrease in κ_T with temperature. In contrast, the three

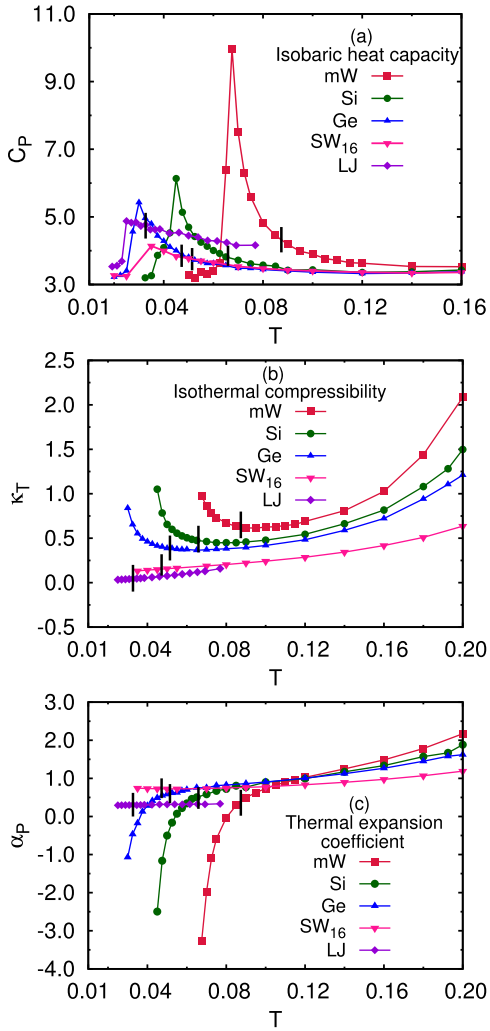

FIG. 2. Thermodynamic response functions on isobaric cooling for Stillinger-Weber (SW) and Lennard-Jones (LJ) liquids: (a) heat capacity, C_P, (b) isothermal compressibility, κ_T, and (c) thermal expansion coefficient, α_P. Stillinger-Weber liquids were cooled along reduced pressure of $P = 3.2269\times10^{-5}$ (equivalent to 1 atm in mW unit) and Lenard-Jones liquid along $P = 1.95$. Melting temperatures in reduced units for each system are shown with black vertical line (|) and correspond to $T_m^{LJ} = 0.850$, $T_m^{SW16} = 0.0472$, $T_m^{Ge} = 0.0514$, $T_m^{Si} = 0.0659$, and $T_m^{mW} = 0.0874$. Corresponding threshold temperatures are $T_{thr}^{SW16} = 0.0350$, $T_{thr}^{Ge} = 0.0300$, $T_{thr}^{Si} = 0.0450$ and $T_{thr}^{mW} = 0.0675$. Melting temperatures are taken from the Refs. 19, 26, 27, 32, and 47. For SW liquids, reduced units are taken to be in terms of well depth, ϵ and size parameter σ of the pair interaction. For the LJ system, C_P, α_P, and κ_T are given in reduced units of ϵ_{LJ} and σ_{LJ}; only temperature for LJ system is reduced in terms of ϵ to ensure that all five systems fall on the same scale.

tetrahedral SW liquids show a pronounced rise or divergence in κ_T as T_{thr} approaches. As tetrahedrality increases (Ge < Si < mW), both T_{thr} and the degree of divergence show a clear increase. It is interesting to note that between the two simple liquids, SW_{16} shows a slightly greater value of κ_T reflecting the more open bcc crystal structure, as opposed to fcc for LJ.

Figure 2(c) shows the thermal expansion coefficient, $\alpha_P(T)$, on isobaric cooling. The two pair-dominated fluids do not show any regime with $\alpha_P < 0$, unlike the three tetrahedral liquids. The point at which the isobaric $\alpha_P(T)$ curve crosses zero lies on the locus of temperatures of maximum density (TMD) curve. For mW, Ge, and Si along the 3.2269 $\times 10^{-5}$ isobar, the T_{TMD} values are given in Table I and show a clear rise with increasing tetrahedrality. The T_{TMD} curve marks the boundaries of the region of density anomaly and has been computed previously for several SW liquids.[20,26]

We now discuss the excess entropy changes associated with supercooling of the Lennard-Jones liquid and the four Stillinger-Weber liquids (see Figure 3). Focusing first on the

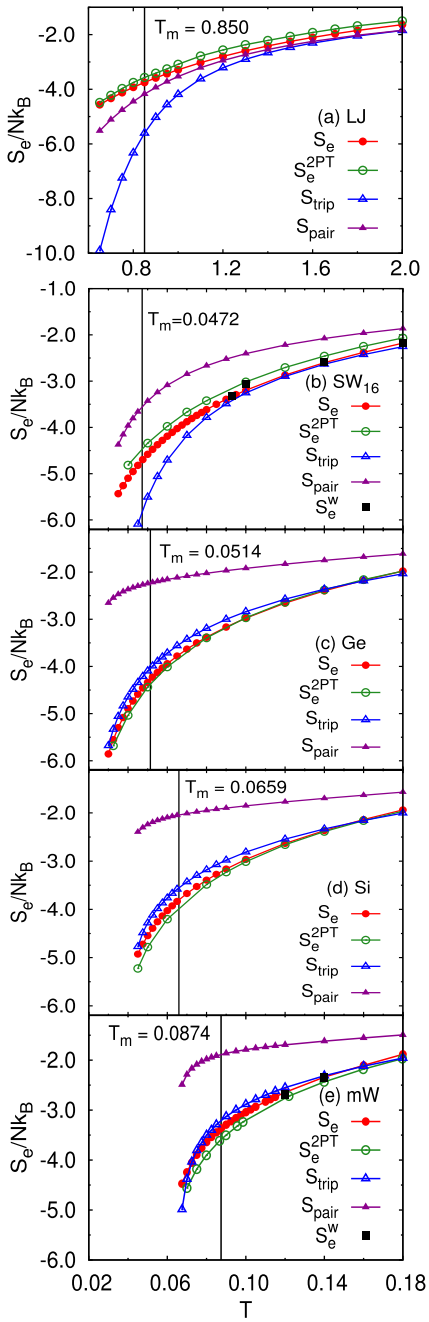

FIG. 3. Excess entropy per particle, S_e as a function of temperature, T for (a) LJ, (b) SW_{16}, (c) germanium (SW_{20}), (d) silicon (SW_{21}), and (e) monatomic water ($SW_{23.15}$). The excess entropy values evaluated by thermodynamic integration (TI), two-phase thermodynamic (2PT) method, and multiparticle correlation expansion (MCE) approximation are compared. The data for Lennard-Jones liquid are along P = 1.95 isobar and for Stillinger-Weber liquids are along $P = 3.2269\times10^{-5}$ isobar. Excess entropy obtained by Widom insertion method for SW_{16} and mW is shown with black squares (■). Melting temperature for each system is indicated with a vertical black line. For SW liquids, reduced units are taken to be in terms of well depth, ϵ and size parameter σ of the pair interaction and for LJ liquid, reduced units are taken to be in terms of ϵ_{LJ} and σ_{LJ}.

excess entropy as evaluated by thermodynamic integration, it is evident that S_e is a smooth function of T as long as the liquid phase remains metastable, i.e., $T \geq T_{thr}$. As the tetrahedrality increases, the slope and curvature of the $S_e(T)$ plots increase in accordance with the heat capacity behaviour but otherwise there are no qualitative differences between water-like and simple fluids.

We now compare the temperature dependent behaviour of the thermodynamic excess entropy, S_e, with the 2PT approximation denoted by S_e^{2PT}. Figure 3(a) shows that for the LJ liquid, S_e^{2PT} lies just above S_e. Figure 3(b) shows that this is also true for the pair-dominated SW_{16}. Interestingly, there is remarkably good agreement between S_e and S_e^{2PT} for germanium melt (SW_{20}). As λ increases, S_e^{2PT} shows small, increasing, negative deviations from S_e. As the discussion in Section II C shows, S^{2PT} is the sum of contributions from a pair-dominated hard-sphere fluid and a set of solid-like, harmonic phonon modes. One expects that the effect of excluded volume effects will be captured to a considerable extent by the hard-sphere component. The fact that S_e^{2PT} approximates the excess entropy very well for both the simple and tetrahedral liquids suggests that the harmonic, phonon-modes provide a reasonable parameterization for capturing the effects of local anisotropy, as it varies from locally icosahedral to tetrahedral. The latter point, however, requires more careful testing in future work.

The two MCE-based approximations to the excess entropy, S_{pair} and S_{trip}, can now be compared with S_e and S_e^{2PT}. Figure 3(a) shows that for the LJ fluid, S_{pair} slightly underestimates S_e until the melting point approaches, when the negative deviations from S_e increase. S_{trip} shows much more pronounced negative deviations from S_e with decreasing temperature. The overall excess entropy, S_e, does not reflect the steep, temperature-dependence of S_{pair} and S_{trip}, originating specially from S_3. This suggests that in the supercooled regime, the higher-order correlation contributions to the entropy, $S_{n>3}$, act to increase the disorder in the system rather to decrease; this maybe due to development of intermediate range bond orientational ordering prior to crystallization.[44] Other thermodynamic and structural consequences of these differences in behaviour of S_2, S_3, and $S_{n>3}$ terms are discussed below. Figures 3(b)-3(e) show comparison of S_{pair} and S_{trip} with S_e^{2PT} and S_e for the four SW liquids.

The striking feature is that S_{trip} provides a remarkably good approximation to the excess entropy for all the

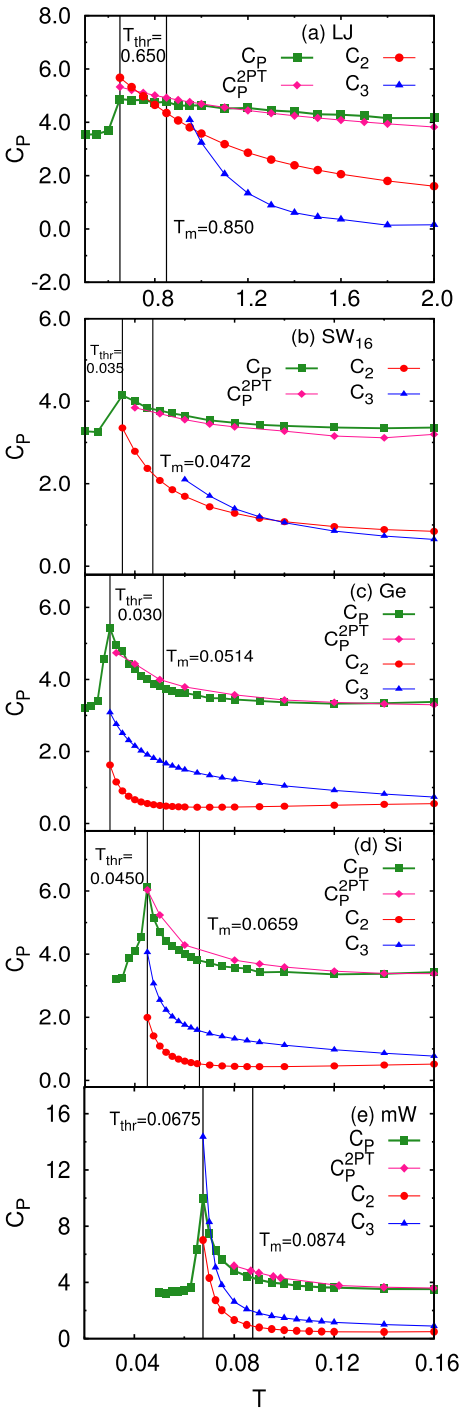

FIG. 4. Heat capacity, C_P as a function of temperature for (a) LJ, (b) SW_{16}, (c) germanium (SW_{20}), (d) silicon (SW_{21}), and (e) monatomic water ($SW_{23.15}$). The data for Lennard-Jones liquid are along P = 1.95 isobar and for Stillinger-Weber liquids are along $P = 3.2269 \times 10^{-5}$ isobar. Heat capacity obtained from two-phase thermodynamic method, C_P^{2PT}, pair and triplet contribution to the heat capacity, C_2 and C_3, respectively, is compared. The heat capacity data for SW_{16} and mW are taken from the literature.[32] Melting temperature (T_m) and threshold temperature (T_{thr}) are shown using a vertical black line. For SW liquids, reduced units are taken to be in terms of well depth, ϵ and size parameter σ of the pair interaction and for LJ liquid, reduced units are taken to be in terms of ϵ_{LJ} and σ_{LJ}.

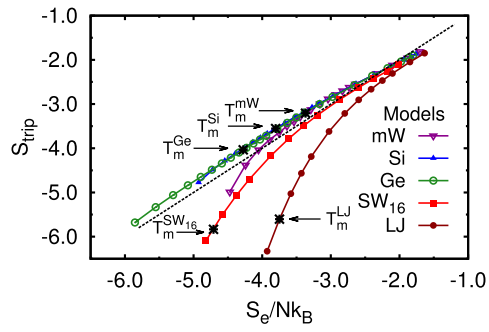

FIG. 5. Correlation between thermodynamic excess entropy, S_e and excess entropy as a sum of pair and triplet contribution, S_{trip}, in Lennard-Jones liquid along P = 1.95 isobar and Stillinger-Weber liquids along $P = 3.2269 \times 10^{-5}$ isobar. Black dashed line is a guide to the eye for the line of slope = 1 and the points (∗) indicate the melting temperature for corresponding systems, $T_m^{LJ} = 0.850$, $T_m^{SW16} = 0.0472$, $T_m^{Ge} = 0.0514$, $T_m^{Si} = 0.0659$, and $T_m^{mW} = 0.0874$ taken from Refs. 19, 26, 27, 32, and 47.

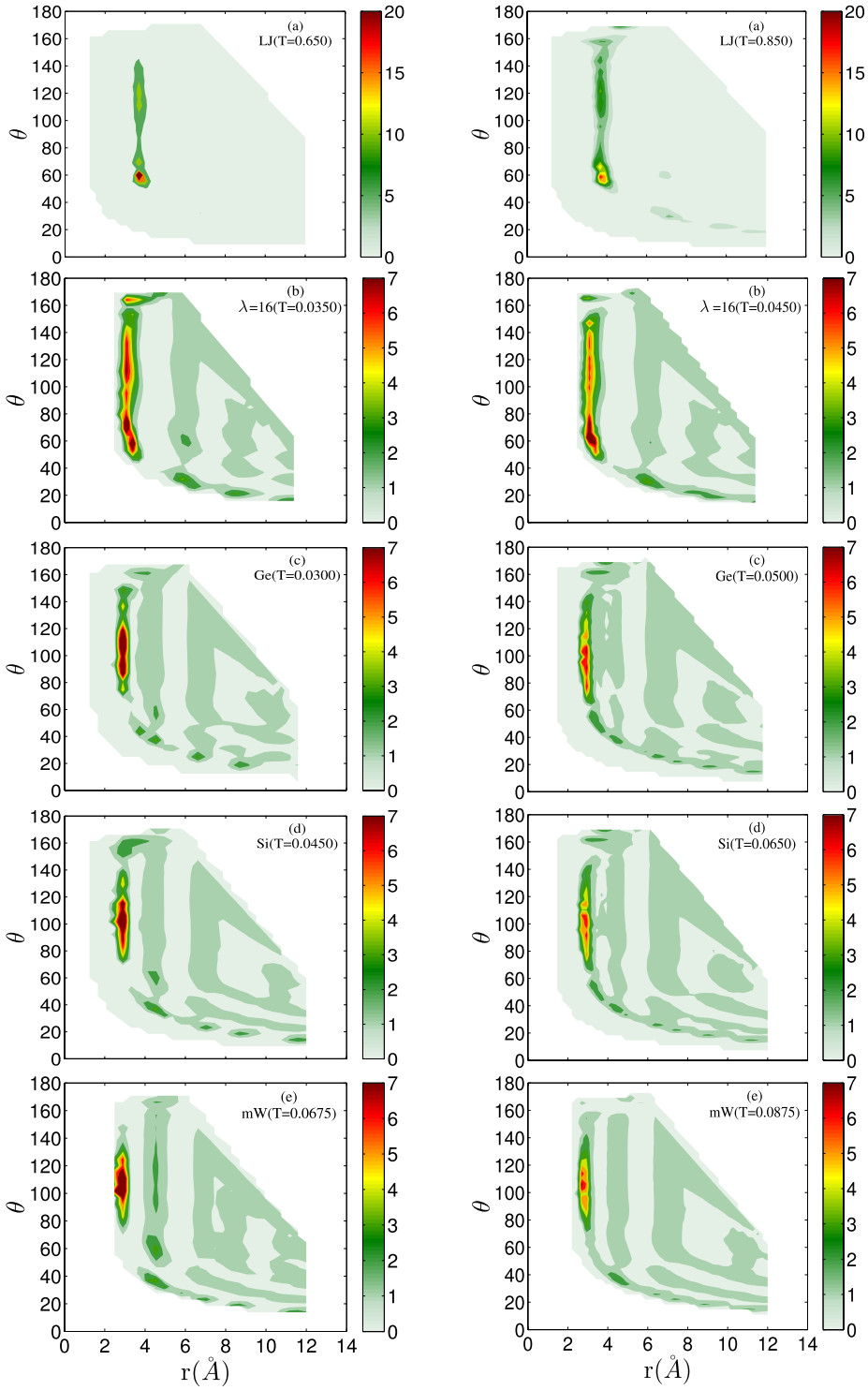

FIG. 6. Contour plots showing isosceles triplet correlation function, $g^{(3)}(r,r,s)$ as a function of distance r and angle θ such that $s^2 = 2r^2(1-\cos\theta)$ for Lennard-Jones liquid at pressure, $P = 1.95$ and Stillinger-Weber liquids at $P = 3.2269\times10^{-5}$: (a) LJ, (b) SW_{16}, (c) germanium (SW_{20}), (d) silicon (SW_{21}), and (e) monatomic water ($SW_{23.15}$). All figures in the left column are at threshold temperature (T_{thr}) for corresponding systems, and the figures in the right column are as close to the melting temperature (T_m).

tetrahedral liquids; for germanium, the agreement between S_e, S_e^{2PT}, and S_{trip} is remarkable. For all the SW liquids, including the pair-dominated SW_{16} system, S_{pair} overestimates S_e by a very significant amount, specially in the supercooled regime. Thus, even though both LJ and SW_{16} are pair-dominated fluids, as indicated, for example, by the response function behaviour, the small differences in the nature of underlying correlations show up both in differences in applicability of the S_{trip} approximation in the supercooled regime.

The qualitative and quantitative differences between triplet-dominated, tetrahedral liquids and pair-dominated, simple liquids with regard to supercooling and crystallization are particularly well-illustrated by the heat capacity behaviour, as illustrated in our previous study contrasting the behaviour of the mW ($SW_{23.15}$) model and the SW_{16} fluid. Here, we extend the data by showing in Figures 4(a)-4(e), the total C_P, C_P^{2PT}, C_2, and C_3 [see Eqs. (11), (39), and (25)] for all five fluids. The heat capacity anomaly of tetrahedral liquids originates in local ordering due to both pair and triplet correlations. This is most pronounced for the mW peak where both the sharp heat capacity rise and excess entropy behaviour are almost entirely captured by the pair and triplet correlations, but is

also clearly present in Ge and Si melt. The anomalous rise in heat capacity on isobaric cooling in tetrahedral fluids can thus be attributed almost entirely to the collective reorganization of the liquid structure due to increasing strength of pair and triplet correlations. In contrast, the pair-dominated liquids show increasing triplet correlations on approaching crystallization but no sharp rise in either the pair or thermodynamic heat capacities. As discussed in our previous study,[32] these triplet correlations have long-range structure which limits the quality of convergence of the triplet entropy and may be associated with the development of long-range bond orientational order.[44,45] Interestingly, the fact that long-range ordering effects show in S_{trip} and C_3, but not in S_e and C_P, is consistent with the mismatch in local order on crystallization of simple liquids. It suggests that on supercooling, local ordering within the first neighbour shell increases significantly, which is expected to be well captured by pair and triplet correlations. In contrast, in tetrahedral liquids, there is no mismatch in local order between the liquid and crystal and development of tetrahedral order on supercooling can proceed unhindered. Moreover, the stronger the tetrahedral bias of the potential, the more pronounced the collective reorganization reflected, for example, in the response function anomalies. It should be noted, however, that even though alternate forms of local ordering, such as pentagonal rings, can exist in tetrahedral liquids,[91] they do not hinder the monotonic increase in tetrahedral order.

A convenient illustration of the differences in the contribution of pair and triplet correlations to thermodynamic behaviour associated with crystallization is provided by the correlation between S_{trip} and S_e (see Figure 5). Molten germanium and silicon show almost perfect correlation between S_{trip} and S_e till T_{thr}, which implies that higher-order particle correlations play a negligible role in these fluids. In the case of mW water, there is a small deviation just below T_m indicating the role of multiparticle correlations close to crystallization. For both the simple liquids, deviations of the slope from unity begin well before the melting point is reached, possibly reflecting the development of bond orientational order as well as higher order correlations discussed earlier. It is an interesting open question whether the lack of higher-order correlations in Ge and Si is connected with their location in the glass-forming, eutectic regime of the Stillinger-Weber phase diagram.

Since triplet correlation functions are, in principle, accessible from scattering experiments, it is useful to document changes in these functions.[92–94] The isosceles triplet correlation functions are particularly convenient for illustrating the changes in local, orientational order accompanying supercooling, specially within the first neighbour shell.[32,89] The isosceles triplet correlation function, $g^{(3)}(r,r,s)$, is the probability of finding three particles with mutual distances such that two distances (r) are equal and the third distance s is given by $s^2 = 2r^2(1 - cos\theta)$. Figure 6 shows the contour plots of $g^{(3)}(r,r,s)$ close to the melting temperature (T_m) and at threshold temperatures (T_{thr}) for all five fluids, which provides an indication of the nature of reorganization of the fluid prior to crystallization. In the case of the Lennard-Jones liquid, at both temperatures, the orientational peak is at 60°, but the disorder in the first neighbour shell appreciably decreases on supercooling, with formation of the fcc crystal resulting in a sharp peak at 60°. The SW_{16} liquid close to T_m shows a significant angular spread with a preference for angles between 50° and 80° as well as broad peak centred at approximately 109°. At T_{thr}, however, the orientational disorder is considerably reduced and there are clearly two peaks at 60° and 70° but the broad peak centred around 109° shrinks only marginally. The pure bcc crystal shows a sharp peak at 70° while the 60° angle is consistent with both fcc and local icosahedral order. The three tetrahedral water-like fluids show angular distributions peaked at ≈109° with progressive localization around the tetrahedral angle with decreasing temperature and increasing tetrahedrality.

V. CONCLUSION

This study uses molecular dynamics simulations to contrast the supercooling and crystallization behaviour of monatomic liquids that exemplify the transition from simple to anomalous tetrahedral liquids. As examples of simple fluids, we use the Lennard-Jones liquid and a pair-dominated Stillinger-Weber liquid (SW_{16}). As examples of tetrahedral, water-like fluids, we use the Stillinger-Weber models for germanium (SW_{20}), silicon (SW_{21}), and monatomic water ($SW_{23.15}$).

The thermodynamic response functions show clear qualitative differences between simple and water-like liquids. For the two simple liquids, the compressibility and the heat capacity are small where quantitative differences may be due to effective softness of pair interactions between the LJ and SW_{16} liquids. The tetrahedral liquids, in contrast, show a very sharp rise in these two response functions as the lower limit of liquid-phase stability is reached, with the extent of divergence as well as the temperature of divergence (T_{thr}) increasing with increasing tetrahedrality when measured in reduced units. While the thermal expansion coefficient decreases with temperature but never crosses zero in simple liquids, in all three tetrahedral liquids at the studied pressure, there is a TMD below which α_P is negative; in reduced units, TMD increases with increasing tetrahedrality. In contrast to the thermodynamic response functions, the excess entropy on isobaric cooling does not show qualitatively different features for simple and water-like liquids; however, the slope and curvature of the $S_e(T)$ plots reflect the heat capacity trends. As a consequence, simple liquids show very little change in the thermodynamic S_e and C_P values on cooling. In contrast, the divergence in the C_P values on cooling due to the heat capacity anomaly in tetrahedral liquids implies a very sharp fall in $S_e(T)$, specially at high tetrahedralities.

The 2PT estimator for the excess entropy proves to be fairly accurate in comparison to the S_e values obtained by thermodynamic integration, for both Lennard-Jones and Stillinger-Weber liquids. To our knowledge, this is one of the few comparisons of the 2PT with TI approaches that are exact, within statistical error, for a given potential model for a fluid.[73,77,95] The 2PT method is remarkably accurate for germanium melt but does not display a significant difference in accuracy between simple and tetrahedral liquids. This suggests that the phonon modes included in the 2PT entropy formulation are able to account for different types of local anisotropy. However,

a further analysis of the 2PT method to extract additional structural insights into the entropy of fluids would be worthwhile.

Two estimators based on the multiparticle correlation expansion of the entropy applicable to incompressible fluids are tested here: S_{pair} and S_{trip}, where the former accounts only for pair correlations whereas the latter accounts for both pair and triplet correlations. For germanium melt, the agreement between S_e, S_e^{2PT}, and S_{trip} is remarkable. For all the SW liquids, including the pair-dominated SW_{16} system, S_{pair} overestimates S_e by a very significant amount, specially in the supercooled regime. Thus, even though both LJ and SW_{16} are pair-dominated fluids, as indicated, for example, by the response function behaviour, the small differences in the nature of underlying correlations are reflected in the MCE evaluation of the excess entropy.

This study confirms our earlier observations that the supercooling and crystallization of tetrahedral liquids are strongly dominated by the local, triplet-dominated reorganisation of the liquid. Since local tetrahedral order is compatible with both liquid and crystalline states, the reorganisation of the liquid is accompanied by a clear rise in the pair, triplet, and thermodynamic contributions to the heat capacity, resulting in the heat capacity and compressibility anomalies. The stronger the energetic bias towards tetrahedrality, the greater the reorganisation on supercooling and therefore the more pronounced the divergence in heat capacity on cooling. In contrast, the pair-dominated liquids show increasing triplet correlations on approaching crystallization but no sharp rise in either the pair or thermodynamic heat capacities. It would be interesting to explore whether this rise in triplet correlations may be associated with the development of long-range bond orientational order.[44,45] Interestingly, the fact that the triplet correlation contribution to the heat capacity and entropy increase in simple liquids despite the overall thermodynamic values of these quantities remaining almost constant suggests that higher-order correlations contribute to increase in disorder in these systems, consistent with the mismatch in local order on crystallization of simple liquids.

Recent studies of complex fluids of patchy colloids, particularly DNA-coated nanocolloids, have opened up the possibility of studying systems with variable tetrahedrality, with interesting similarities and differences with the Stillinger-Weber fluids studied here.[96–99] Since light-scattering techniques can be used to obtain pair and triplet correlation information on these systems,[92–94] the multiparticle correlation expansion of the entropy holds interesting possibilities in understanding phase transitions in these systems.

ACKNOWLEDGMENTS

C.C. would like to thank Department of Science and Technology, New Delhi for financial support. D.D. and P.K. would like to thank University Grants Commission, New Delhi for the award of senior research fellowships. A.H.N. would like to thank Tod A. Pascal for the 2PT code. Computational resources for this study were provided by the High Performance Computing facility of the Indian Institute of Technology Delhi. V.M. and A.H.N. acknowledge support from the U.S. National Science Foundation through Award No. CHE-1309601.

[1]J.-L. Barrat and J.-P. Hansen, *Basic Concepts for Simple and Complex Liquids* (Cambridge University Press, 2003).
[2]J.-P. Hansen and I. R. McDonald, *Theory of Simple Liquids: With Applications to Soft Matters* (Academic Press, 2013).
[3]D. Nayar and C. Chakravarty, Phys. Chem. Chem. Phys. **15**, 14162 (2013).
[4]A. K. Bacher, T. B. Schrøder, and J. C. Dyre, Nat. Commun. **5**, 5424 (2014).
[5]L. Bøhling, T. S. Ingebrigtsen, A. Grzybowski, M. Paluch, J. C. Dyre, and T. B. Schrøder, New J. Phys. **14**, 113035 (2012).
[6]T. S. Ingebrigtsen, A. A. Veldhorst, T. B. Schrøder, and J. C. Dyre, J. Chem. Phys. **139**, 171101 (2013).
[7]P. G. Debenedetti, J. Phys.: Condens. Matter **15**, R1669 (2003).
[8]J. R. Errington and P. G. Debenedetti, Nature **409**, 318 (2001).
[9]C. A. Angell and H. Kanno, Science **193**, 1121 (1976).
[10]C. A. Angell, P. A. Cheeseman, and S. Tamaddon, Science **218**, 885 (1982).
[11]P. H. Poole, M. Hemmati, and C. A. Angell, Phys. Rev. Lett. **79**, 2281 (1997).
[12]C. A. Angell, R. D. Bressel, M. Hemmati, E. J. Sare, and J. C. Tucker, Phys. Chem. Chem. Phys. **2**, 1559 (2000).
[13]R. Sharma, S. N. Chakraborty, and C. Chakravarty, J. Chem. Phys. **125**, 204501 (2006).
[14]B. S. Jabes, M. Agarwal, and C. Chakravarty, J. Chem. Phys. **132**, 234507 (2010).
[15]M. Wilson, Phys. Chem. Chem. Phys. **14**, 12701 (2012).
[16]A. S. Barnard and S. P. Russo, Mol. Phys. **100**, 1517 (2002).
[17]F. H. Stillinger and T. A. Weber, Phys. Rev. B **31**, 5262 (1985).
[18]S. Sastry and C. A. Angell, Nat. Mater. **2**, 739 (2003).
[19]V. Molinero, S. Sastry, and C. A. Angell, Phys. Rev. Lett. **97**, 075701 (2006).
[20]V. V. Vasisht, S. Saw, and S. Sastry, Nat. Phys. **7**, 549 (2011).
[21]F. Sciortino, Nat. Phys. **7**, 523 (2011).
[22]M. H. Bhat, V. Molinero, E. Soignard, V. C. Solomon, S. Sastry, J. L. Yarger, and C. A. Angell, Nature **448**, 787 (2007).
[23]M. Posselt and A. Gabriel, Phys. Rev. B **80**, 045202 (2009).
[24]I. Saika-Voivod, F. Romano, and F. Sciortino, J. Chem. Phys. **135**, 124506 (2011).
[25]Y. Wang, Y. Wang, D. R. Breed, V. N. Manoharan, L. Feng, A. D. Hollingsworth, M. Weck, and D. J. Pine, Nature **491**, 51 (2012).
[26]W. Hujo, B. S. Jabes, V. K. Rana, C. Chakravarty, and V. Molinero, J. Stat. Phys. **145**, 293 (2011).
[27]V. Molinero and E. B. Moore, J. Phys. Chem. B **113**, 4008 (2009).
[28]B. S. Jabes, D. Nayar, D. Dhabal, V. Molinero, and C. Chakravarty, J. Phys.: Condens. Matter **24**, 284116 (2012).
[29]V. Holten, D. T. Limmer, V. Molinero, and M. A. Anisimov, J. Chem. Phys. **138**, 174501 (2013).
[30]S. Sengupta, V. V. Vasisht, and S. Sastry, J. Chem. Phys. **140**, 044503 (2014).
[31]V. V. Vasisht, J. Mathew, S. Sengupta, and S. Sastry, J. Chem. Phys. **141**, 124501 (2014).
[32]M. Singh, D. Dhabal, A. H. Nguyen, V. Molinero, and C. Chakravarty, Phys. Rev. Lett. **112**, 147801 (2014).
[33]M. Wilson and P. F. McMillan, Phys. Rev. Lett. **90**, 135703 (2003).
[34]P. Beaucage and N. Mousseau, J. Phys.: Condens. Matter **17**, 2269 (2005).
[35]E. B. Moore and V. Molinero, J. Chem. Phys. **130**, 244505 (2009).
[36]E. B. Moore and V. Molinero, J. Chem. Phys. **132**, 244504 (2010).
[37]E. B. Moore and V. Molinero, Nature **479**, 506 (2011).
[38]L. C. Jacobson, R. M. Kirby, and V. Molinero, J. Phys. Chem. B **118**, 8190 (2014).
[39]F. Romano, T. K. J. Russo, and H. Tanaka, Phys. Rev. B **90**, 014204 (2014).
[40]A. Haji-Akbari, M. Engel, A. S. Keys, X. Zheng, R. G. Petschek, P. Palffy-Muhoray, and S. C. Glotzer, Nature **462**, 773 (2009).
[41]G. V. Anders, D. Klotsa, N. K. Ahmed, M. Engel, and S. C. Glotzer, Proc. Natl. Acad. Sci. U. S. A. **111**, E4812 (2014).
[42]P. J. Steinhardt, D. R. Nelson, and M. Ronchetti, Phys. Rev. Lett. **47**, 1297 (1981).
[43]P. J. Steinhardt, D. R. Nelson, and M. Ronchetti, Phys. Rev. B **28**, 784 (1983).
[44]H. Tanaka, J. Stat. Mech.: Theory Exp. **2010**, P12001.
[45]H. Tanaka, Eur. Phys. J. E **35**, 113 (2012).
[46]D. T. Limmer and D. Chandler, J. Chem. Phys. **135**, 134503 (2011).
[47]M. A. Barroso and A. L. Ferreira, J. Chem. Phys. **116**, 7145 (2002).
[48]Y. Rosenfeld, Phys. Rev. A **15**, 2545 (1977).
[49]Y. Rosenfeld, J. Phys.: Condens. Matter **11**, 5415 (1999).
[50]B. S. Jabes and C. Chakravarty, J. Chem. Phys. **136**, 144507 (2012).
[51]S. Prasad and C. Chakravarty, J. Chem. Phys. **140**, 164501 (2014).
[52]M. D. Allen and D. J. Tildesley, *Computer Simulation of Liquids* (Oxford University Press, New York, 1989).
[53]D. Frenkel and B. Smit, *Understanding Molecular Simulation: From Algorithms to Applications* (Academic Press, 2002).

[54]M. E. Tuckerman, *Statistical Mechanics: Theory and Molecular Simulation* (Oxford University Press, New York, 2010).
[55]M. Karplus and J. N. Kushick, Macromolecules **14**, 325 (1981).
[56]I. Andricioaei and M. Karplus, J. Chem. Phys. **115**, 6289 (2001).
[57]J. Schlitter, Chem. Phys. Lett. **215**, 617 (1993).
[58]H. Schäfer, A. E. Mark, and W. F. van Gunsteren, J. Chem. Phys. **113**, 7809 (2000).
[59]S. T. Lin, M. Blanco, and W. A. Goddard III, J. Chem. Phys. **119**, 11792 (2003).
[60]S. T. Lin, P. K. Maity, and W. A. Goddard III, J. Phys. Chem. B **114**, 8191 (2010).
[61]B. J. Borah, P. K. Maiti, C. Chakravarty, and S. Yashonath, J. Chem. Phys. **136**, 174510 (2012).
[62]S. K. Sinha, M. Jana, K. Chakraborty, and S. Bandyopadhyay, J. Chem. Phys. **141**, 22D502 (2014).
[63]H. S. Green, *The Molecular Theory of Fluids* (North-Holland Publishing Co., Amsterdam, 1952).
[64]H. J. Raveché, J. Chem. Phys. **55**, 2242 (1971).
[65]R. D. Mountain and H. J. Raveché, J. Chem. Phys. **55**, 2250 (1971).
[66]A. Baranyai and D. J. Evans, Phys. Rev. A **40**, 3817 (1989).
[67]D. C. Wallace, J. Chem. Phys. **87**, 2282 (1987).
[68]A. Baranyai and D. J. Evans, Phys. Rev. A **42**, 849 (1990).
[69]B. B. Laird and A. D. J. Haymet, Phys. Rev. A **45**, 5680 (1992).
[70]T. Arisawa, T. Arai, and I. Yokoyama, Physica B **262**, 190 (1999).
[71]J. R. Errington, T. M. Truskett, and J. Mittal, J. Chem. Phys. **125**, 244502 (2006).
[72]S. N. Chakraborty and C. Chakravarty, J. Chem. Phys. **124**, 014507 (2006).
[73]S. N. Huang, T. A. Pascal, W. A. Goddard III, P. K. Maiti, and S. T. Lin, J. Chem. Theory Comput. **7**, 1893 (2011).
[74]T. A. Pascal, D. Schärf, Y. Jung, and T. D. Kühne, J. Chem. Phys. **137**, 244507 (2012).
[75]B. Jana, S. Pal, P. K. Maiti, S. T. Lin, J. T. Hynes, and B. Bagchi, J. Phys. Chem. B **110**, 19611 (2006).
[76]T. A. Pascal, S. T. Lin, and W. A. Goddard III, Phys. Chem. Chem. Phys. **13**, 169 (2011).
[77]P. K. Lai, C. M. Hsieh, and S. T. Lin, Phys. Chem. Chem. Phys. **14**, 15206 (2012).
[78]T. A. Pascal and W. A. Goddard III, J. Phys. Chem. B **118**, 5943 (2014).
[79]B. Widom, J. Chem. Phys. **39**, 2808 (1963).
[80]A. K. Soper, Mol. Phys. **99**, 1503 (2001).
[81]A. K. Soper, J. Phys.: Condens. Matter **17**, S3273 (2005).
[82]A. K. Soper, J. Phys.: Condens. Matter **19**, 335206 (2007).
[83]K. T. Wikfeldt, M. Leetmaa, A. Mace, A. Nilsson, and L. G. M. Pettersson, J. Chem. Phys. **132**, 104513 (2010).
[84]K. T. Wikfeldt, M. Leetmaa, M. P. Ljungberg, A. Nilsson, and L. G. M. Pettersson, J. Phys. Chem. B **113**, 6246 (2009).
[85]B. B. Laird and A. D. J. Haymet, J. Chem. Phys. **97**, 2153 (1992).
[86]N. F. Carnahan and K. E. Starling, J. Chem. Phys. **53**, 600 (1970).
[87]S. Plimpton, J. Comput. Phys. **117**, 1 (1995), see http://lammps.sandia.gov.
[88]W. J. McNeil, W. G. Madden, A. D. J. Haymet, and S. A. Rice, J. Chem. Phys. **78**, 388 (1983).
[89]D. Dhabal, M. Singh, K. T. Wikfeldt, and C. Chakravarty, J. Chem. Phys. **141**, 174504 (2014).
[90]M. Singh, "Relationships between structure, entropy and mobility in simple and anomalous liquids," Ph.D. thesis, School of Physical Sciences, JNU, New Delhi, 2014.
[91]J. Russo and H. Tanaka, Nat. Commun. **5**, 3556 (2014).
[92]K. Zahn, G. Maret, C. Ruß, and H. H. von Grüunberg, Phys. Rev. Lett. **91**, 115502 (2003).
[93]P. A. Egelstaff, D. I. Page, and C. R. T. Heard, Phys. Lett. A **30A**, 376 (1969).
[94]P. A. Egelstaff, D. I. Page, and C. R. T. Heard, J. Phys. C: Solid State Phys. **4**, 1453 (1971).
[95]J. Wang, B. Chakraborty, and J. Eapen, Phys. Chem. Chem. Phys. **16**, 3062 (2014).
[96]B. Ruzicka, E. Zaccarelli, L. Zulian, R. Angelini, M. Sztucki, A. Moussaïd, T. Narayanan, and F. Sciortino, Nat. Mater. **10**, 56 (2010).
[97]F. Smallenburg, L. Filion, and F. Sciortino, Nat. Phys. **10**, 653 (2014).
[98]S. Biffi, R. Cerbino, G. Nava, F. Bomboi, F. Sciortino, and T. Bellini, Soft Matter **11**, 3132 (2015).
[99]J. Lu, Y. Qiu, R. Baron, and V. Molinero, J. Chem. Theory Comput. **10**, 4104 (2014).